

AD-A154 118

EMISSION FROM CO2 AROUND 27 MICROMETERS FROM DAYLIGHT
ATMOSPHERES(U) ARCON CORP WALTHAM MA R D SHARMA ET AL.
21 JAN 85 AFGL-TR-85-0045 F19628-84-C-0017

1/1

UNCLASSIFIED

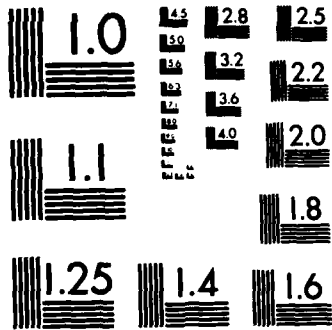
F/G 4/1

NL

END

FORM

DEC



MICROCOPY RESOLUTION TEST CHART
NATIONAL BUREAU OF STANDARDS-1963-A

EMISSION FROM CO₂ AROUND 2.7 MICROMETERS
FROM DAYLIT ATMOSPHERES

21 January 1985

Ramesh D. Sharma
Infrared Technology Division
Air Force Geophysics Laboratory
Hanscom A. F. B., MA 01731

Peter P. Wintersteiner
ARCON Corporation
260 Bear Hill Road
Waltham, MA 02154

AD-A154 118

AD-A154 118

ABSTRACT

Micrometers

A detailed study of the vibrational states of CO₂ in the upper atmosphere was conducted in order to enable the calculation of emission near 2.7 μ m expected for sunlit conditions. New line-by-line computer codes were used to evaluate the solar pumping of vibrational levels and to calculate the limb radiance. Excitation and quenching mechanisms are quantified and limb radiance is computed for several important vibrational transitions in the altitude range 60-100 km. The dominance of fluorescent CO₂ hot band emission for altitudes below 75 km is confirmed. The spectral distribution, and to a lesser degree the total band radiance, are shown to be very sensitive to collisional interactions. Detailed results are presented and compared with experiment.

Originator supplied keywords include:

1. INTRODUCTION

Daytime upper-atmosphere emission in the near infrared may be the result of resonant and fluorescent transitions directly following excitation of vibrational states of molecules by the absorption of solar flux. In this paper we report the results of a modelling effort which predicts the daytime emission from CO₂ in the 2.7 μ m region. This prediction is facilitated by a careful calculation of the populations of radiating states. In addition to the population of the upper states by solar photons, and quenching due to collisions with N₂ molecules, the calculation includes other collisional excitation and quenching mechanisms which turn out to be important.

The first step in our calculation is the determination of solar flux absorption coefficients for the various bands which populate the radiating states of interest. The second step consists of the evaluation of the steady-state populations of sets of excited states, using the various excitation and quenching mechanisms. The sets were delimited by the extent to which the states within them are coupled by collisional interactions. The final calculation is that of the resulting emission, as seen by a hypothetical exoatmospheric sensor in limb-looking geometry. Both the absorption and emission calculations were performed with new line-by-line computer codes which properly account for the absorption occurring along the paths.

1

UNCLASSIFIED

DTIC FILE COPY

This document has been approved for public release and sale; its distribution is unlimited.

DTIC ELECTE
MAY 24 1985

A

DDI 473
Block 18

Unclassified

SECURITY CLASSIFICATION OF THIS PAGE

REPORT DOCUMENTATION PAGE

1a. REPORT SECURITY CLASSIFICATION Unclassified		1b. RESTRICTIVE MARKINGS	
2a. SECURITY CLASSIFICATION AUTHORITY		3. DISTRIBUTION/AVAILABILITY OF REPORT Approved for public release; Distribution unlimited.	
2b. DECLASSIFICATION/DOWNGRADING SCHEDULE			
4. PERFORMING ORGANIZATION REPORT NUMBER(S) AFGL-TR-85-0045		5. MONITORING ORGANIZATION REPORT NUMBER(S)	
6a. NAME OF PERFORMING ORGANIZATION Air Force Geophysics Laboratory	6b. OFFICE SYMBOL (If applicable) LSI	7a. NAME OF MONITORING ORGANIZATION	
6c. ADDRESS (City, State and ZIP Code) Hanscom AFB Massachusetts 01731		7b. ADDRESS (City, State and ZIP Code)	
8a. NAME OF FUNDING/SPONSORING ORGANIZATION	8b. OFFICE SYMBOL (If applicable)	9. PROCUREMENT INSTRUMENT IDENTIFICATION NUMBER	
8c. ADDRESS (City, State and ZIP Code)		10. SOURCE OF FUNDING NOS.	
		PROGRAM ELEMENT NO. 61102F	PROJECT NO. 2310
		TASK NO. G4	WORK UNIT NO. 20
11. TITLE (Include Security Classification) EMISSION FROM CO₂ Around 2.7 Micrometers From Daylit Atmospheres			
12. PERSONAL AUTHOR(S) Ramesh D. Sharma; Peter P. Wintersteiner*			
13a. TYPE OF REPORT REPRINT	13b. TIME COVERED FROM _____ TO _____	14. DATE OF REPORT (Yr., Mo., Day) 1985 March 13	15. PAGE COUNT 17
16. SUPPLEMENTARY NOTATION *ARCON Corp, 260 Bear Hill Rd, Waltham, MA 02154 Presented at the Meeting of the IRIS Specialty Group on Targets, Backgrounds & Discrimination, Naval Training Ctr, Orlando, FL, 12-14 February 1985			
17. COSATI CODES		18. SUBJECT TERMS (Continue on reverse if necessary and identify by block number)	
FIELD	GROUP	SUB. GR.	
		Infrared solar pumping, Carbon Dioxide Emission.	
19. ABSTRACT (Continue on reverse if necessary and identify by block number) A detailed study of the vibrational states of CO ₂ in the upper atmosphere was conducted in order to enable the calculation of emission near 2.7µm expected for sunlit conditions. New line-by-line computer codes were used to evaluate the solar pumping of vibrational levels and to calculate the limb radiance. Excitation and quenching mechanisms are quantified and limb radiance is computed for several important vibrational transitions in the altitude range of 60-100 km. The dominance of fluorescent CO ₂ hot band emission for altitudes below 75 km is confirmed. The spectral distribution, and to a lesser degree the total band radiance, are shown to be very sensitive to collisional interactions. Detailed results are presented and compared with experiment.			
20. DISTRIBUTION/AVAILABILITY OF ABSTRACT UNCLASSIFIED/UNLIMITED <input type="checkbox"/> SAME AS RPT. <input checked="" type="checkbox"/> DTIC USERS <input type="checkbox"/>		21. ABSTRACT SECURITY CLASSIFICATION Unclassified	
22a. NAME OF RESPONSIBLE INDIVIDUAL Ramesh D. Sharma		22b. TELEPHONE NUMBER (Include Area Code) 617-861-2261	22c. OFFICE SYMBOL AFGL/LSI

One of the reasons for undertaking this study was the existence of data from the rocket-borne SPIRE experiment, which observed infrared emission over a wide range of wavelengths in the Arctic near sunrise on Sept. 28, 1977. Details of the execution and principal results of this experiment are given elsewhere¹⁻³. An earlier study⁴ has found that the daytime emission detected by the SPIRE sensor near $2.7\mu\text{m}$ contains, primarily, contributions from the ν_1 and ν_3 fundamentals of water vapor and the 101 combination bands of CO_2 . In the latter case it was also established that solar pumping of the 201 and 301 levels followed by fluorescence to 100 and 200, respectively, gives a more significant component of the CO_2 emission than the resonant 101--000 transitions. This and other conclusions of the earlier work are confirmed in the present effort, and additional contributions from other bands are evaluated as well. Several collisional excitation and quenching mechanisms which were not previously considered have been included here, and their effect is assessed. The inclusion of these collisional mechanisms decreases the observed emission by only about 30%. However, it markedly changes the spectral distribution of the observed radiance.

2. CALCULATION OF VIBRATIONAL-LEVEL POPULATIONS

Before the $2.7\mu\text{m}$ emission from CO_2 can be computed, the steady-state populations of all the radiating levels must be calculated. Figure 1 is an energy level diagram for the principal (626) isotope showing the vibrational states which are necessary for this calculation. The $2.7\mu\text{m}$ transitions, including solar pumping from the ground state, are indicated by the solid lines. The important solar pumping at 2.0 and $1.6\mu\text{m}$ is also indicated. Four groups of high-lying levels, including all the levels radiating at $2.7\mu\text{m}$, are identified. Within each group the vibrational levels are strongly coupled by collisional interactions. The principal radiating levels are $1001x$ ($x=1,2$) in Group 1; $1111x$ ($x=1,2$) in Group 2; $2001y$ ($y=1,2,3$) in Group 3; and $3001z$ ($z=1,2,3,4$) in Group 4. The notation for the vibrational levels is standard AFGL notation⁵, as is the isotopic designation.

Table 1 lists the 26 bands in the $2.7\mu\text{m}$ region whose contribution to the total radiance has been calculated in this modelling effort. These bands are divided into eight sets, A through G, to facilitate our discussion.

The only mechanisms which couple states within any single group are collisional interactions which cause small changes in the internal energy of the CO_2 molecule and reorient the vibrational motion. These result from collisions with air molecules, whose internal energy states remain unchanged.

1. Stair, A. T., Jr., Sharma, R. D., Nadile, R. M., Baker, D. J., and Grieder, W. F., "Observations of Limb Radiance with Cryogenic Spectral Infrared Rocket Experiment (SPIRE), to be published.
2. Sharma, R. D., "Infrared Airglow", in Handbook of Geophysics, Chapter 13 (in press).
3. Nadile, R. M., Wheeler, N. B., Stair, A. T., Jr., Prodsham, D. C. and Wyatt, L. C., "SPIRE Spectral Infrared Experiment," SPIE 24 - Modern Utilization of Infrared Technology, 18-24, 1977.
4. Sharma, R., Nadile, R., Stair, A. T., Jr., and Gallery, W., "Earthlimb Emission Analysis of Spectral Infrared Rocket Experiment (SPIRE) Data at 2.7 Micrometers," SPIE 304 - Modern Utilization of Infrared Technology, 139-142, 1981.
5. McClatchey, R. A., Benedict, W. S., Clough, S. A., Burch, D. E., Calfee, R. F., Fox, K., Rothman, L. S., and Garing, J. S., "AFGL Atmospheric Absorption Line Parameters Compilation," AFGL-TR-73-0096 (1973), NTIS #AD762904.

UNCLASSIFIED

2



85 04 24 05

UNCLASSIFIED

The individual states within each group are also coupled to other (lower lying) CO₂ states by the absorption and emission of radiation, mostly at 2.7 μ m and 4.3 μ m, and by exchange of vibrational quanta with N₂ molecules⁶⁻⁸. The latter process, the net effect of which is usually to quench CO₂ 2.7 μ m emission, involves a change of ± 1 in the ν_2 quantum number. In general, then, radiative transitions near 4.3 μ m are in parallel with collision-induced V-V transitions coupling the same vibrational levels. The populations of the lower-lying states, which are needed to calculate excitation rates, are taken to be static. This is a reasonable approximation, as these levels are more strongly coupled to each other than to the higher lying levels in which we are primarily interested. The static populations that we used were obtained through the courtesy of T. Degges of Visidyne Corp. from a simulation of the conditions of the SPIRE experiment using the A.F.G.L. High-Altitude Infrared Radiance Model (IRR). It turns out that the lower-lying excited states are important for our calculations only at altitudes below 60 km. In this altitude range our static populations are practically the same as LTE populations.

Table 2 lists the collisional reorientation reactions which couple the states of group 1 to each other, and the V-V interactions which couple them to lower-lying states. The reactions involving states of the other three groups are completely analogous.

The four groups of states are treated as independent of each other. This is a good approximation because the possible transitions between states in different groups are very much weaker than other transitions involving them. That is, because of larger energy differences, collisional transfer rates are lower between groups than within groups. The most important radiative transitions between groups, ν_2 transitions, turn out to be a minor perturbation in the overall picture.

In order to calculate the steady-state populations of vibrational levels within a group, one simply equates the sum of excitation rates for each level with the sum of de-excitation rates for that level. To exemplify some of the pertinent considerations, we briefly discuss the 10012 state alone, and then a group of states (10012, 02211, 10011) which were treated simultaneously.

In the simplest view, 10012 is populated by solar pumping from the ground state, quenched by collisions with ground-state nitrogen and additionally depleted by spontaneous radiation in the 4.3 μ m and 2.7 μ m bands. This picture is complicated slightly by the recognition that, with a sufficiently large population in the low-lying 10002 level, excitation of 10012 may occur because of collisions with excited-state nitrogen and also because of solar pumping in the 4.3 μ m band. From this, the desired number density can be calculated by equating the rates of solar pumping of 10012 from ground and 10002 plus the excitation rate due to V-V interactions with

6. Sharma, R. D. and Brau, C. A., "Energy Transfer in Near-Resonant Molecular Collisions due to Long-Range Forces with Application to Transfer of Vibrational Energy from ν_2 Mode of CO₂ to N₂", J. Chem. Phys. **50**, 924 (1969).
7. Kumer, J. B. and James, T. C., "CO₂(001) and N₂ Vibrational Temperatures in the 50 z 130 km Altitude Range," J. Geophys. Res., **79**, 638 (1974).
8. Kumer, J. B., "Atmospheric CO₂ and N₂ Vibrational Temperature at 40- to 140-km Altitude," J. Geophys. Res., **82**, 2195 (1977).
9. Degges, T. and Smith, H.J.P., "A High-Altitude Infrared Radiance Model," AFGL-TR-77-0271 (1977).

UNCLASSIFIED

UNCLASSIFIED

the sum of the rates for spontaneous emission and for quenching due to V-V interactions.

Because of the expected strong collisional coupling of the 10012 level with the 02211 and 10011 levels, this simple picture is inadequate to determine the population of 10012. One must identify the important collisional interactions, put in collisional rate constants, and solve simultaneous equations for the populations of all three levels. The effect of doing this is noteworthy in two important respects.

First of all, the discussion, above, of the 10012 level also applies to 10011 to the extent that one can ignore collisional coupling. The 02211 level, however, is different because its radiative transitions to and from the ground level, and to and from 01101, are forbidden. As a result, what population there is comes from absorption of solar photons around $4.3\mu\text{m}$ by the thermally populated state (02201) at 1335 cm^{-1} . The pumping is therefore much weaker than that for the other two levels. The mechanisms for quenching emission at $2.7\mu\text{m}$, on the other hand, consist of V-V interactions with nitrogen molecules and radiation at $4.3\mu\text{m}$, and are comparable in strength to those of the other two levels. The result, then, of coupling 02211 to 10012 and 10011 is to provide a pathway whose net effect is to deplete the populations of the latter two states. (At least, this is true for altitudes at which a sufficient number of collisions occur to couple these states effectively.)

The second notable effect of coupling the levels within this group is to deplete the higher-lying levels (e.g., 10011) in favor of the lower-lying ones. This causes a larger fraction of the emitted radiation to appear at $2.77\mu\text{m}$ —and a smaller fraction at $2.69\mu\text{m}$ —than would otherwise be the case, and thus affects the distribution of radiation in the wavelength region under consideration. In general, the levels split by Fermi-resonance—levels differing only in the fifth index—are probably coupled to each other much more strongly than to the other nearby levels such as 02211, which have a different symmetry. (We call these other levels "side levels" for want of a better term.) They are therefore likely to be in equilibrium with each other at quite high altitudes, considerably higher than the altitudes at which they are effectively decoupled from the "side levels".

The three equations which need to be solved for the number densities of the states of Group 1 are inhomogeneous coupled linear equations and are easily solved by matrix inversion. The inhomogeneous terms represent excitation from the lower-lying states, whose populations are presumed fixed. The matrix elements are derived from the rate constants describing the collisional interactions and the V-V interactions, and from the Einstein coefficients governing spontaneous emission.

The three other groups of states are treated in a similar manner. Each level of each group is coupled to all other levels in its own group by collisional processes. Solar pumping of all allowed transitions from ground and low-lying thermally populated levels is the principal excitation mechanism of the high-lying states. Excitation by V-V interactions with N_2 is included for states of groups 2 and 3 but is much less important than for those of group 1. De-excitation mechanisms are the same as for group 1: spontaneous emission and quenching by collisions with N_2 .

UNCLASSIFIED

UNCLASSIFIED

3. TRANSMISSION CALCULATIONS

New computer codes were used to compute the transmission of radiation through the absorbing non-LTE atmosphere. The objective of program SABS is to calculate coefficients of absorption of solar flux for each of several bands which contribute to the excitation of the radiating states. These coefficients, given in units of photons per second per molecule of CO₂ for altitudes down to 40 km, are converted into band excitation rates by multiplying by the CO₂ number density. The excitation rates contribute to the calculation of the vibrational populations, as described in the previous section. Program NLTE¹⁰ uses the vibrational populations to evaluate the volume emission rate at different altitudes and compute the observed radiance at the end of specified viewing paths.

Both programs are line-by-line codes drawing on the data collected in the A.F.G.L. Atmospheric Absorption Line Parameters Compilation^{5,11}. Within each band the lines are assumed to be independent (no overlap), so the total absorption in the band, and the total radiance at the end of the viewing path, are just the sum of the contributions from all the lines. For each line in the band, both codes trace the absorption (and, in the case of NLTE, the emission) of flux through the atmosphere along the viewing path at selected frequencies between the line center and the wings, thereby producing transmission lineshapes at each altitude. These profiles are sufficiently detailed to permit numerical integration over frequency, yielding the total absorption (SABS) or radiance (NLTE) for the line.

The basic idea behind NLTE is to divide the atmosphere into concentric layers having uniform atmospheric properties and, for each frequency within each line, evaluate the photon flux on the line-of-sight path at the edge of each layer. That is, a certain flux is incident on the layer, and a certain flux emanates from within it. The program calculates the contribution from within the layer, with attenuation accounted for by integration over the layer, and also the amount of flux transmitted completely through the layer. The sum of these is the flux seen at the opposite edge of the layer on the viewing path, and this serves as the flux incident on the next layer. The calculation proceeds from layer to layer, starting at the top of the atmosphere (where the incident flux is zero), passing through the tangent point, and proceeding out again to the top of the atmosphere where the observer is presumed to sit.

To find the emission and absorption at each frequency within a line, it is necessary to know the upper and lower rotational state populations, and the line-shape. The latter is specified by a Voigt function, and the former are calculated from the vibrational populations and the information on the A.F.G.L. database by using a rotational temperature equal to the kinetic temperature. The two main datasets required for this calculation, therefore, are the properties of all the transitions in the band and the atmospheric profile specifying temperature, number densities, and pressure as a function of altitude. Reference 10 describes the algorithm

10. Sharma, R. D., Siani, R., Bullitt, M., and Wintersteiner, P. P., "A Computer Code to Calculate Emission and Transmission of Infrared Radiation through a Non-Equilibrium Atmosphere," AFGL-TR-83-0168 (1983), NTIS #ADA137162.
11. Rothman, L. S., Gamache, R. R., Barbe, A., Goldman, A., Gillis, J. R., Brown, L. R., Toth, R. A., Flaud, J. M., and Camy-Payret, C., "AFGL Atmospheric Absorption Line Parameters Compilation: 1982 Edition," App. Opt. 22, 2247 (1983).

UNCLASSIFIED

UNCLASSIFIED

in some mathematical detail. The atmospheric layers were taken to be 1 km thick and spanned the altitude range from the tangent point to 160 km.

SABS differs from NLTE in that it simply evaluates the attenuation of solar flux rather than calculating a continuous emission and absorption along the path. The upper-state vibrational and rotational populations are therefore irrelevant. The viewing path and the incident flux at the top of the atmosphere are also different. We used a standard solar-flux profile¹² and a solar elevation angle of 12°, which closely corresponds to the conditions of the first daylight scan of the SPIRE experiment. The atmospheric layers were 1 km thick between 40 and 160 km. In other respects the procedures and assumptions used in NLTE are applied in SABS as well.

4. RESULTS FOR SOLAR ABSORPTION COEFFICIENTS AND CO₂ VIBRATIONAL LEVEL POPULATIONS

In this section we briefly outline the results of the solar-flux absorption and CO₂ vibrational population calculations discussed in the previous two sections, and give examples of the sort of information which is derived from them. Results of the radiance calculations are given in Sections 5 and 6.

Figure 2 gives the solar-flux absorption coefficients as a function of altitude for transitions which populate states in Group 1, for the major isotope and for the 636 isotope. It illustrates the point that while the greatest absorption usually occurs in bands originating in the ground state, hot bands do not always give negligible contributions.

The absorption which occurs along the paths used to calculate these curves ranges from negligible ("thin" lines) to severe ("thick" lines) to extreme. A convenient figure of merit, τ_c , is the optical depth (at a given altitude) at the center of the strongest line of a band, from which one can crudely estimate the attenuation by comparing its value with unity.

The two uppermost curves in Figure 2, giving the transitions up from ground to the 1001x levels, exhibit the full range of possibilities. At the highest altitudes the curves are nearly flat because the CO₂ density is too low to significantly deplete the incident radiation. Between 100 and 55 km the solar excitation drops by two orders of magnitude because of the severe absorption taking place in this region. The optical depth parameter, τ_c , at these two altitudes is approximately .1 and 200, respectively. The extreme case is illustrated by the upturn near 50 km. This occurs because of absorption in the wings of the Voigt lines, which become more prominent because of collision-broadening. At these altitudes the flux at the line-centers is completely absorbed out but because of the small collision width at greater altitudes, that in the wings is not diminished at all. Thus, the increasing breadth of the absorption lineshape is responsible for the increase in absorption, which now occurs far from the line centers. This behavior of course does not occur when a Doppler lineshape is used to describe the cross-sections; rather, the monotonic decrease with decreasing altitude is maintained below 60 km for all reasonable temperature profiles.

For the other bands originating in the ground state, the onset of severe

12. Thekaekara, M. P., *Solar Energy* 14, 109 (1973), summarized in Houghton, J. T., *The Physics of Atmospheres*, Cambridge, Univ. Press, 1977.

UNCLASSIFIED

attenuation occurs at lower altitudes, reflecting weaker transitions, or, in the case of minor isotopes, smaller ground-state populations.

The differences between the 10012 and 10011 curves occur because of different transition strengths. Attenuation of solar photons has the effect of equalizing the pumping rates at lower altitudes, but at higher altitudes these differences strongly affect the vibrational level populations and thus the distribution of radiation in the $2.7\mu\text{m}$ window. This consideration is very important for the 2001y states of group 3, because 20012 is pumped much more strongly than 20011 and 20013.

Given the solar-pumping results, it is straightforward to set up and solve the equations for the populations of the levels of the four chosen groups. The results for the states of group 1 are given in Figure 3, as the ratio of their number densities to that of the ground state. In Figure 4, we break out the separate excitation and de-excitation rates for the 10012 level in the 40-100 km altitude region. Similar curves, not shown, were calculated for states other than those of Group 1.

5. RESULTS FOR LIMB RADIANCE

The most important result of this paper is presented in Figure 5, which gives the total integrated radiance in the $2.7\mu\text{m}$ region as a function of the tangent height of the line-of-sight path, and also breaks it down into contributions from the sets of bands identified in Table 1. It is clear from these curves that the dominant contribution at high altitudes comes from the resonant transitions, set A, while at low altitudes the fluorescent bands of set B, bands involving transitions 2001y-1000x, are the most important component. (Their contributions are equal for the path with a tangent-height of approximately 77 km.) Next in importance are the bands of set C, and the resonant bands of the minor isotopes, summed (set G). Set D gives 10% of the total for the 60 km path but drops rapidly in importance with increasing altitude, as do all bands whose upper states are populated primarily as a result of collisions. The two lowest curves, resulting from states in Group 4, contribute at most 2% of the total and need not be considered. In addition, the 2001y-1000x bands of the minor isotopes, not shown, fall in the range between these last two curves.

The radiance contributed by the major-isotope resonant bands, set A, changes very little over the range of line-of-sight paths because self-absorption is important even for the highest paths. On the 100 km path, for which these bands comprise 90% of the total radiance, the optical depth parameters, τ_c , are about 1.3 and 2.0 for 10012-00001 and 10011-00001, respectively, and the actual contributions are greater than for the 60 km path. All the other bands have only thin lines on the 100 km path, and their contributions simply reflect the upper-state populations, which of course decrease rapidly with increasing altitude. In fact, the only other bands for which self-absorption plays an important role at any altitude above 60 km are the minor-isotope resonance bands, set G, and the major-isotope 1111x-01101 hot bands of set C, whose lower state is only 667 cm^{-1} above ground. At 60 km the largest τ_c value for any band in set B is about .5, which implies a little attenuation along that path.

One can see from Figure 5 that between 60 and 75 km it is important to consider at least five contributions to the total radiance. No single family comprises more

UNCLASSIFIED

UNCLASSIFIED

than 45% of the total in this altitude range. On the 60 km path the contributions from sets B, A, C, G, and D are 45%, 16%, 13%, 13% and 11% respectively; for the 75 km path they are 37%, 28%, 15%, 14% and 5%.

Figures 6 and 7 give the spectral distribution of radiation between 2.6 μ m and 2.9 μ m. In order to obtain this, the NLTE output for each line was convolved with an instrumental scanning function appropriate to the SPIRE experiment. The lines were approximated by delta functions with amplitudes equal to the integrated radiance. A triangular scanning function with a FWHM of 52 cm^{-1} , or .038 μ m was used to simulate the effect of this instrument.

Figure 6 gives the total predicted spectral radiance from all the CO₂ bands for paths with tangent heights between 60 and 100 km. One notable feature is that the relative size of the two peaks changes substantially with tangent height. This occurs because of the diminishing importance, with increasing altitude, of collisional excitation and de-excitation mechanisms as compared with radiative mechanisms. That is, collisions have the effect of diminishing the population of higher-lying levels within each group and enhancing that of the lower ones, and the net result for lower altitudes is more radiation at longer wavelengths. On the other hand, at 100 km the radiative excitation and de-excitation mechanisms stand alone and (because the pumping to the 10011 level is more likely than that to 10012, as mentioned earlier) the shorter-wavelength peak is larger for paths that traverse regions near and above this altitude.

Another point worth noting is the shifting of the longer-wavelength peak from about 2.80 μ m to about 2.77 μ m as the tangent-height increases from 60 to 100 km. This is a result of the decreasing importance of two of the fluorescent bands in set B, which peak at slightly longer wavelengths, when compared to the resonant band at 2.77 μ m. The shorter-wavelength peaks are more nearly coincident.

Figure 7 gives a breakdown of the total spectral radiance seen on the 75 km path by sets of bands, including only the five most prominent contributions. It is interesting to note that the long-wavelength tail of the distribution ($\lambda > 2.85\mu$ m) is primarily determined by the minor-isotope emission.

6. MODIFICATIONS TO THE BASIC MODEL

In order to assess quantitatively the effects of including the intragroup collisional interactions, we performed the vibrational-population and radiance calculations using alternative values for the rate constants.

The first modification (Mod1) consisted of setting those rate constants which couple the side levels to the principal radiating levels---e.g., k_{12} in Table 2---equal to zero. This has the effect of eliminating the influence of these levels (02211 in Group 1; 03311 in Group 2; 12211, 12212, and 04411 in Group 3; 22211-22213 in Group 4) on the vibrational population calculations.

In modification number 2 (Mod2) the rate constants coupling the Fermi-resonance split states---e.g., k_{13} in Table 2---as well as those coupling them to the side levels were set equal to zero, thereby making all levels of each group independent of all others. This results in calculations which are most like those previously reported⁴.

Modification number 3 (Mod3) is the same as the basic model, except that the rate constants connecting the Fermi-resonance split levels were increased by a

UNCLASSIFIED

UNCLASSIFIED

factor of 100. These levels are thereby coupled more strongly to each other.

Figures 8 and 9 summarize the overall effect of making these alterations by plotting, respectively, the total radiance as a function of tangent height and the $2.7\mu\text{m}$ spectral radiance for the 75 km tangent-height path, each calculated under the assumptions of the basic model and those of Mod1 and Mod2. Mod3 produces radiances which hardly differ from those of the basic model.

Two things become clear from comparing the results of the basic model to those of Mod1 and Mod2. First of all, the rate at which collisions redistribute the populations of the Fermi-resonance split levels among themselves has a great influence not only on the spectral distribution, but also on the total emission. Secondly, the decoupling of the side levels has the anticipated effect of increasing the emission from the principal radiating levels, but it is by an amount which is considerably less than that resulting from decoupling all the levels. A more detailed examination of the results reveals that the principal differences between the Mod2 curves and the others comes from much greater populations of, and hence emission from, certain states of Group 3, primarily 20012.

The most general conclusion that can be drawn is that the observed radiance depends very strongly on the collisional interactions among the high-lying states, and that it is very important to know the rate constants for the reactions coupling these states.

To see how the changes depicted in Figures 8 and 9 arise, we examine Mod1 and Mod2 in more detail. Mod1 decouples the side levels completely and removes a quenching mechanism for the more important radiating states. In Figure 3, the dashed line gives the populations of Group 1 states under these assumptions. It shows that above the altitude (approximately 55 km) where N_2 excitation is unimportant the 02211 state is not highly populated. The 1001x populations are augmented by as much as 20% between 60 and 80 km, but the limb radiance resulting from them is increased by a smaller percent because of self-absorption. In Group 2, the 1111x populations are augmented by 15% or less.

Mod1 strongly affects the populations of the 2001y states of Group 3, with increases of 80% at some altitudes and appreciable effects all the way from 40 to 90 km. This more dramatic response to the decoupling of the side levels reflects the lower excitation rates and the greater number of quenching channels (compared to the 1001x levels) for these states. The change in the total limb radiance from the basic model is mostly due to these augmented populations, and occurs despite the near-complete elimination of the contribution from the bands of set D originating in the 1221x side levels.

The Mod1 spectral distribution is not significantly different from that of the basic model.

The second modification---namely, decoupling all the high-lying states from each other---has very important implications. In Mod1 the Fermi-resonance split states are still strongly coupled, so the additional limitation imposed by Mod2 results only in the redistribution of the populations of the excited states, compared to Mod1. One would thus expect little change in the total emission from Mod1 to Mod2. This neglects, however, the important fact that the states which are most strongly coupled to ground---and which therefore are more strongly pumped---may

UNCLASSIFIED

radiate more (or less) strongly in their respective $2.7\mu\text{m}$ bands than other states in the same group. The absence of the collisional redistribution will therefore result in more (or less) total emission from these states. This is a pertinent consideration for the 1001x levels and the 2001y levels. In fact, the Einstein A coefficient for the transition to ground of the 10011 level (16.9 sec^{-1}) is about 50% greater than that of the 10012 level (11.0 sec^{-1}), so (as can be seen from Figure 2 above 90 km) the solar pumping of this level is greater and also the probability of radiation at $2.7\mu\text{m}$ from this level is greater. Since this level is actually depleted in favor of 10012 by collisional interactions, the proper result is less emission than is found when (as in Mod2) these levels are assumed to be independent.

The same result holds for the 2001y family of Group 2. Our calculations show that for altitudes at which attenuation of sunlight is unimportant the 20012 level is much more strongly pumped than the other two. It happens that the total Einstein coefficient for emission at $2.7\mu\text{m}$ from 20012 is greater than that of the lower-lying 20013 (18.1 sec^{-1}) and higher-lying 20011 (33.5 sec^{-1}). The net effect of decoupling these levels, then, is to keep the more weakly-radiating lowest level from acquiring the large population collecting in the middle and upper levels. Mod2 therefore predicts a considerably greater total emission near $2.7\mu\text{m}$ than the basic model, as shown in Figure 8. This result calls attention to the need to carefully consider the collisional interactions.

Figure 9 shows that the changes which constitute Mod2 give a strikingly different spectral distribution from that of the basic model. This occurs because of the greater weighting Mod2 accords the higher-lying states, which radiate more prominently in shorter-wavelength bands.

Mod3 is, in some sense, the opposite of Mod1 and Mod2 because it couples the principal radiating states more, rather than less, strongly. The quantitative result is that the populations are weighted slightly more heavily toward the lower vibrational levels, as one would expect. Below 85 km the population differences are too small to be seen on the logarithmic scale of Figure 2. Above 85 km the redistribution is more obvious. By the converse of the logic employed in the discussion of Mod2 in the last two paragraphs, one expects this to reduce the observed radiation. This turns out to be the case, but since emission from Group 3 is relatively unimportant above 85 km the limb radiance is not affected dramatically.

7. COMPARISON WITH EXPERIMENTAL RESULTS

The $2.7\mu\text{m}$ emission seen by SPIRE and other experimental probes has components due to molecules other than CO_2 . The most important of these is H_2O , which radiates in four bands between $2.68\mu\text{m}$ and $2.75\mu\text{m}$. The possibility of contributions from the OH fundamental on the long-wavelength side cannot be ruled out, either.

Modelling the water contribution is made difficult by the uncertainty in, and variability of, the mixing ratio for H_2O . Degges et al.¹³ have determined that the SPIRE data at $6.3\mu\text{m}$ and $2.7\mu\text{m}$ for paths with tangent heights up to 75 km are consistent with a mixing ratio of 1.5 parts per million by volume, although higher

13. Degges, T. and Nadile, R., "Determination of Mesospheric Water Vapor Concentrations from Earth Limb Radiance Measurements at 6.3 and 2.7 Micrometers" (to be published).

UNCLASSIFIED

values are not ruled out. He has calculated the H₂O contribution in the 2.5-2.9 μ m region on this basis. In Figure 10 we compare the results of our basic model for CO₂, Degges' results for H₂O, and the total of these quantities with the SPIRE data-set for tangent heights between 50 and 90 km.

Figure 10 shows that below 70 km there is good agreement between the total predicted limb radiance and the experimental values, which do not vary strongly with altitude. Above 75 km the emission falls off rapidly into the range of detector noise. In fact, the data are very noisy at these altitudes, and it is only possible to say that the actual emission must be less than 1.6×10^{-8} watt/cm²-ster, the noise level. Since the CO₂ prediction is less than this, no conclusion can be drawn regarding it. The H₂O prediction of limb radiance is significantly above this for tangent heights between 75 and 85 km, however, a fact that suggests that the correct water vapor mixing ratio over most of the range above 75 km must be less than 1.5 ppm.

Figure 11 presents spectral data in the 2.5-3.5 μ m region, with the background subtracted out. These data correspond to a tangent height of 73 km. We also show the H₂O component and the combined CO₂ and H₂O prediction. The latter provides a respectable representation of the data. It somewhat overestimates the experiment at 2.70 μ m, in the shorter wavelength CO₂ peak (c.f. Figure 6); and it underestimates it on the long-wavelength side of the CO₂ spectrum and beyond. This fit illustrates quite clearly the importance of including the collisional interactions in the CO₂ model. That is, if the results of the basic model were replaced by the Mod2 results (c.f. Figure 9) both the overestimate of the experiment at 2.70 μ m and the underestimate beyond 2.80 μ m would be exaggerated rather than diminished.

It should be pointed out that the water calculation is a band model calculation, and may not represent the spectral distribution as precisely as appears necessary to resolve the discrepancies between the combined model and the experiment in the 2.7-2.8 μ m region.

8. DISCUSSION

It is clear from the discussion of the last two sections that the interactions coupling the states within each of the groups of high-lying states play a major, albeit not dominant, role in determining the CO₂ contribution to the 2.7 μ m radiance. The values of the rate constants used in the basic model, given in Table 2, were chosen to be the same as those coupling the 10001-02201-10002 states in IRR⁹. In fact, k_{13} is the lower limit proposed by Taylor¹⁴ for the rate constant characterizing



These values are not known with great accuracy, and we also do not know exactly what differences can be expected between the constants coupling states of this low-lying group and those characterizing our four high-lying groups. The values used in our basic model thus represent educated guesses of how strong the interactions are. The purpose of making the changes described as Mod1-Mod3 was to crudely evaluate the effect of these guesses on the observed radiance.

14. Taylor, R. L., "Energy Transfer Processes in the Stratosphere," Can. J. Chem. 52, 1436 (1974).

UNCLASSIFIED

UNCLASSIFIED

The effect of reducing k_{13} can be seen, from Mod2, to be to increase the 2.7 μ m emission. If the H₂O contribution predicted by Degges¹³ is correct, the overall fit in the 50-70 km region precludes the possibility of a larger CO₂ component. Thus the value we have used for k_{13} could be a lower limit, in accord with Taylor¹⁴. We have not shown that some lower values are inconsistent with the data, but since k_{13} determines the largest de-excitation rate for the very important 20012 and 20011 states it is likely that modest reductions in its value will lead to larger populations, and therefore greater emission.

Because, in our basic model, the Fermi-resonance split levels are in near equilibrium with each other up to about 85 km, increasing k_{13} (Mod3) has little effect on the emission in the region where good data are found. Above 85 km the reduction in the predicted radiance is less than the uncertainty in the H₂O contribution. For these reasons, it is impossible to decide from this model whether a larger value for k_{13} is appropriate.

The effect of reducing k_{12} is to weaken the coupling between the principal radiating levels and the side levels, and thus to increase the populations of the former. This results in greater emission from them. By reasoning similar to that pertaining to k_{13} , we conclude that the value for k_{12} found in the basic model represents a lower limit. In contrast, larger values cannot be ruled out. An order-of-magnitude increase in k_{12} causes a decrease in emission which removes the overall H₂O-CO₂ prediction from agreement with the experiment. However a larger water mixing ratio---2 ppm in the 50-70 km range, which is still consistent with the SPIRE results in the 6.3 μ m region---could make up the difference. A smaller value of k_{13} might have the same effect.

One result which has not been mentioned can be seen in Figure 4: in a range of altitudes between 42 and 52 km the net effect of collisions between N₂ and CO₂ molecules is to excite, rather than deplete, the 1001x levels of CO₂. Generally this mechanism quenches high-lying CO₂ levels. In this altitude range LTE is believed to prevail for the low-lying levels involved in these transitions (e.g., 1000x, 02201), and the resulting populations happen to be great enough that reactions 4 and 6 in Table 2 run in reverse. One implication of this result is that for paths intersecting this altitude range some 2.7 μ m emission should appear even for night-time conditions. The SPIRE detectors did not observe night-time emission at this wavelength. This is explained by the fact that in the absence of solar pumping our model predicts limb radiances from these bands on the order of 10⁻⁹ watt/cm²-ster, which is well below the noise level of the instruments.

9. CONCLUSION

A model for the prediction of CO₂ emission in the 2.7 μ m region has been developed, and tested by simulating the conditions of the SPIRE experiment. A new line-by-line code has been used to evaluate the rates of absorption of solar flux in many relevant bands. These rates have been combined with assumed rates for inter- and intra-molecular collisional interactions to evaluate the populations of high-lying levels responsible for emission in the 101 combination bands. The limb radiance has been calculated from these populations. In combination with emission from water vapor predicted by another model¹³, it has been compared with the SPIRE dataset for daylight conditions. Rate constants for the intramolecular collisional

UNCLASSIFIED

UNCLASSIFIED

interactions have also been altered to test the effect of possible errors in their values.

In general the model has been found to give good agreement with the experiment. It has also established the need to include the intramolecular collisional interactions in calculating the vibrational populations of the high-lying levels. Among our specific conclusions are that (1) the resonant transitions 1001x-00001 dominate the limb radiance above 75 km; (2) the fluorescent transitions 2001y-1000x are most significant on lower viewing paths, but several other sets of bands, including those of minor isotopes, contribute a sizable portion of the observed radiance; (3) the principal excitation mechanism is solar pumping over the entire range of altitudes considered, even when the line centers are so completely bleached out that absorption occurs primarily in the Voigt wings; (4) the high-lying levels are de-excited primarily through radiative processes above 75 km and through collisions with N_2 below 75 km; (5) the intramolecular collisional transfer rates strongly affect the (integrated) limb radiance and also the spectral shape of the emission; and (6) the values of the rate constants used to characterize these interactions could be adjusted upward without causing conflict with the data, but a significant downward revision appears to inappropriate.

10. ACKNOWLEDGEMENTS

We would like to acknowledge several helpful conversations with T. Degges and also thank him for making his paper on water vapor available prior to publication.

This work was supported by U.S.A.F. contract F19628-84-C-0017. We are grateful for help and support provided by A.F.O.S.R., particularly by D. Ball and T. Cress; and by D.N.A., particularly by K. Schwartz and P. Lunn.

UNCLASSIFIED

UNCLASSIFIED

Set	Band	Isotope	Vib. Transition		A (sec ⁻¹)
			(cm ⁻¹)	(μm)	
A	10012-00001	626	3612.8	2.77	11.0
	10011-00001	626	3714.8	2.69	16.9
	20013-10002	626	3568.2	2.80	18.1
B	20012-10002	626	3692.4	2.71	24.4
	20012-10001	626	3589.7	2.79	16.0
	20011-10001	626	3711.5	2.69	33.5
C	11112-01101	626	3580.3	2.79	10.8
	11111-01101	626	3723.2	2.69	16.5
D	12212-02201	626	3552.9	2.81	10.6
	12211-02201	626	3726.7	2.68	18.1
	30014-20003	626	3527.6	2.83	25.2
E	30013-20003	626	3679.6	2.72	26.1
	30013-20002	626	3556.8	2.81	28.3
	30012-20002	626	3676.7	2.72	43.9
	30012-20001	626	3550.7	2.82	16.1
	30011-20001	626	3705.9	2.70	49.6
F	22213-12202	626	3518.7	2.84	20.0
	22212-12202	626	3703.5	2.70	24.1
	22212-12201	626	3527.8	2.83	12.8
	22211-12201	626	3713.8	2.69	41.4
	10012-00001	636	3527.7	2.83	8.7
	10011-00001	636	3632.9	2.75	15.7
	10012-00001	628	3571.1	2.80	13.5
10011-00001	628	3675.1	2.72	13.1	
10012-00001	627	3590.9	2.78	12.1	
10011-00001	627	3693.6	2.71	15.6	

Table #1 CO₂ vibrational bands whose contributions to the total radiance observed near 2.7μm have been calculated in this study. Bands are grouped into sets A through G to facilitate the discussion.

Collisional Reorientation Reactions	Forward Rate Constant
1. CO ₂ (10011) + M → CO ₂ (10012) + M	$k_{11} = 3 \times 10^{-11}$
2. CO ₂ (02211) + M → CO ₂ (10012) + M	$k_{12} = 1.5 \times 10^{-13}$
3. CO ₂ (10011) + M → CO ₂ (02211) + M	$k_{21} = 2k_{12}$
V-V exchange with N ₂	
4. CO ₂ (10012) + N ₂ (0) → CO ₂ (10002) + N ₂ (1)	$k_v = 5 \times 10^{-13} \left(\frac{300}{T}\right)^4$
5. CO ₂ (02211) + N ₂ (0) → CO ₂ (02201) + N ₂ (1)	
6. CO ₂ (10011) + N ₂ (0) → CO ₂ (10001) + N ₂ (1)	

Table #2 Reactions resulting in non-radiative transitions involving the three states of Group 1. The forward rate constants used in the basic model are also listed. These numerical values for k_{11} and k_{12} were used for analogous reorienting collisional interactions coupling states in Groups 2-4. The same is true of k_v for V-V interactions involving states of Groups 2-4.

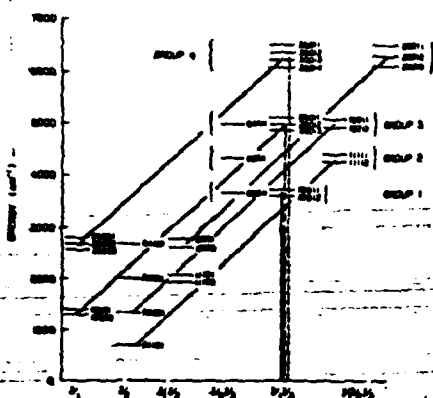


Figure 1. CO₂ energy levels relevant for the 2.7 μm radiance calculations, including the four groups of high-lying states discussed in the text. Solid lines show 2.7 μm radiative transitions. Vertical lines show the principal solar pumping channels. For Group 2, the 2.7 μm resonance bands are the major channels.

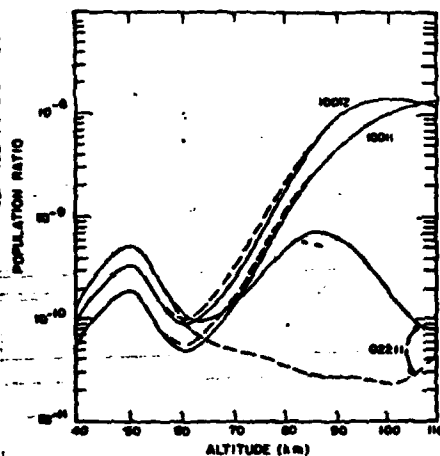


Figure 3. Ratios of the populations of the three vibrational levels in Group 1 to that of the ground state for the 626 isotope. Solid lines give results from the basic model and dashed lines give results from Mod. 1. See Section 6.

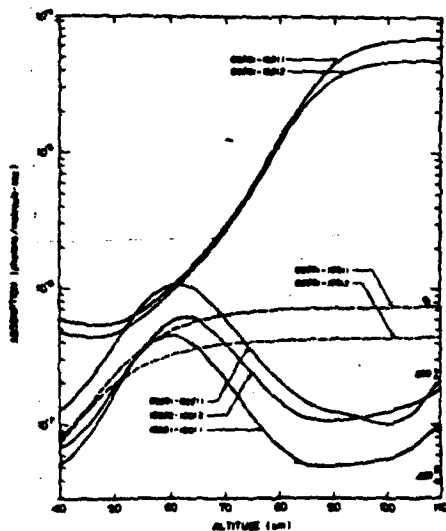


Figure 2. Solar flux absorption coefficients for bands populating states in Group 1. Solid lines refer to the 626 isotope, dashed lines to the 636 isotope. Xs mark the high-altitude limits for absorption in the 2.7 μm bands of the 627 and 628 isotopes.

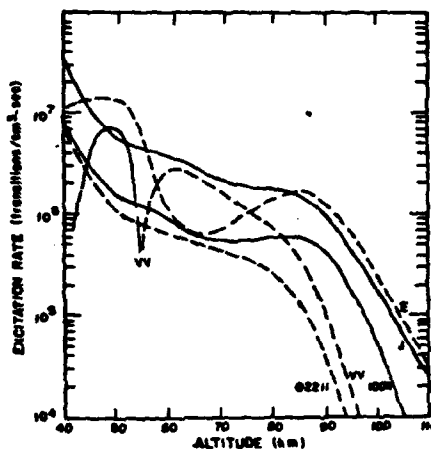


Figure 4. Excitation rates (solid lines) and de-excitation rates (dashed lines) due to mechanisms coupling the 10012 level with other levels. "J" represents solar pumping from lower states, "E" represents spontaneous emission, "VV" represents N₂ collisions and "10011" and "02211" represent collisional interactions with those two levels.

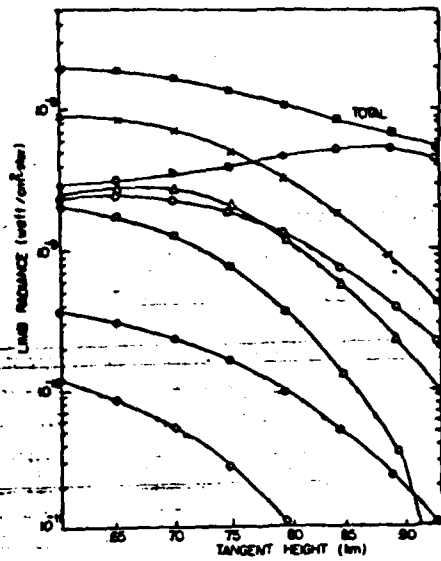


Figure 5. Band radiance in the 2.6-2.9 μm range, as a function of tangent height. Sets of bands are: \odot Set A; \times Set B; Δ Set C; \square Set D; \bullet Set E; \diamond Set F; \circ Set G. See Table 1.

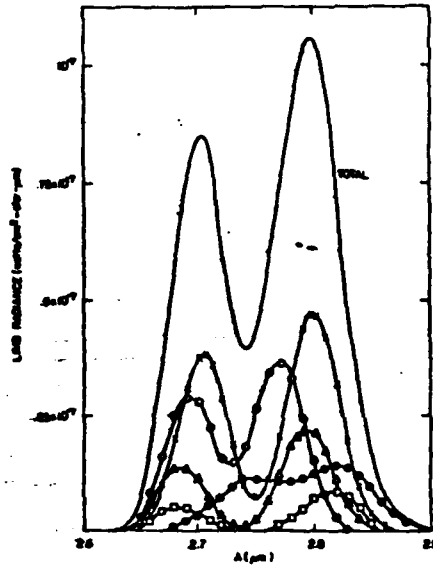


Figure 7. Spectral distribution of limb radiance for the path with a tangent height of 75 km. Components are sets of bands as in Figure 5, except that \odot refers to set G.

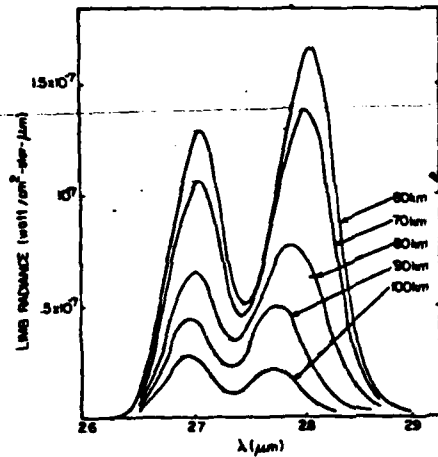


Figure 6. Spectral distribution of limb radiance, from the basic model. Curves refer to tangent heights between 60 and 100 km.

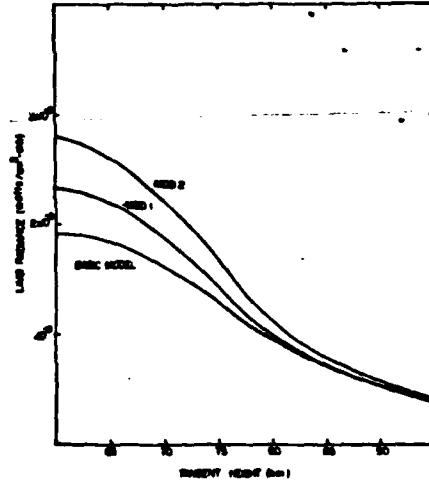


Figure 8. Integrated limb radiance from the basic model and from two modifications, as a function of tangent height.

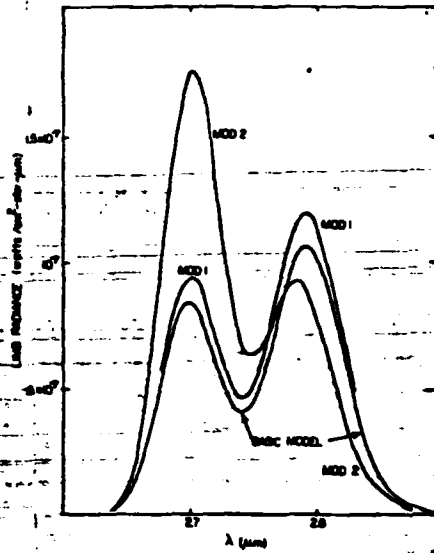


Figure 9. Spectral distribution of limb radiance from the basic model and from two modifications, for a path with a tangent height of 75 km.

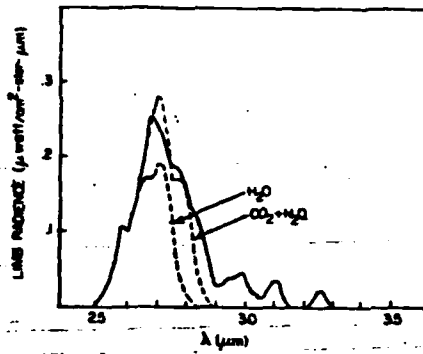


Figure 11. Limb radiance from the SPIRE experiment (solid line) in comparison with predictions of contributions from CO₂ and H₂O.

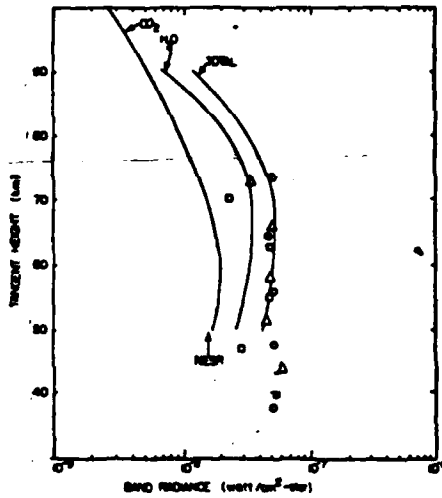


Figure 10. Band radiance, 2.5-2.9 μm, from scans 9 (O), 10 (Δ), and 11 (□) of the SPIRE experiment, and the results of the CO₂ model, the H₂O model, and their total. Detector noise limit is indicated by the arrow.

END

FILMED

7-85

DTIC